Savage, J., Pianosi, F., Bates, P., Freer, J., & Wagener, T. (2016). Quantifying the importance of spatial resolution and other factors through global sensitivity analysis of a flood inundation model. Water Resources Research. DOI: 10.1002/2015WR018198

Quantifying the importance of spatial resolution and other factors through global sensitivity analysis of a flood inundation model

Authors

James Thomas Steven Savage[13*], Francesca Pianosi[23], Paul Bates[13], Jim Freer[13] & Thorsten Wagener[2,3]

[1]School of Geographical Sciences, University of Bristol, Bristol, BS8 1SS, United Kingdom

[2]Department of Civil Engineering, University of Bristol, Bristol, BS8 1TR, United Kingdom

[3]Cabot Institute, University of Bristol, Bristol, BS8 1UJ, United Kingdom

Key Points

Key Point 1: Sensitivity of flood inundation predictions to different input factors shown to be more complex than previously thought

Key Point 2: The most influential model input factor for predicting flood extent changes during the flood event

Key Point 3: Spatial resolution is much more influential for localised predictions of water depth than for flood extent

Abstract

Where high resolution topographic data are available, modellers are faced with the decision of whether it is better to spend computational resource on resolving topography at finer resolutions or on running more simulations to account for various uncertain input factors (e.g. model parameters). In this paper we apply Global Sensitivity Analysis to explore how influential the choice of spatial resolution is when compared to uncertainties in the Manning's friction coefficient parameters, the inflow hydrograph, and those stemming from the coarsening of topographic data used to produce Digital Elevation Models (DEMs).. We apply the hydraulic model LISFLOOD-FP to produce several temporally and spatially variable model outputs that represent different aspects of flood inundation processes, including flood extent, water depth and time of inundation. We find that the most influential input factor for flood extent predictions changes during the flood event, starting with the inflow hydrograph during the rising limb before switching to the channel friction parameter during peak flood inundation, and finally to the floodplain friction parameter during the drying phase of the flood event. Spatial resolution and uncertainty introduced by resampling topographic data to coarser resolutions are much more important for water depth predictions, which are also sensitive to different input factors spatially and temporally. Our findings indicate that the sensitivity of LISFLOOD-FP predictions is more complex than previously thought. Consequently, the input factors that modellers should prioritise will differ depending on the model output assessed, and the location and time of when and where this output is most relevant.

Keywords

Sensitivity Analysis, Sobol' method, Flood inundation modelling, Spatial resolution, Uncertainty, Hydraulic model

Index Terms

1821 Floods (4303), 1847 Modeling (1952, 4316), 1873 Uncertainty assessment (1990, 3275), 1817 Extreme events (4313), 4307 Methods (0500, 3200, 4400) (Within Natural Hazards)

1. Introduction

Flood inundation models have been utilised widely to make flood hazard predictions. These models are typically run in either steady state, where the boundary conditions (for a river this would typically be the river discharge) are fixed in time, or in unsteady state, where the boundary conditions change through time. Steady state models have been applied for various applications, including to undertake flood hazard mapping from reference return period events (e.g. *Cook and Merwade*, 2009) and to compare different hydraulic models (*Bradbrook et al.*, 2004), whilst models run in an unsteady state enable modellers to understand the dynamic variation of flood hazard throughout the passage of the flood wave (e.g. *Bates and De Roo*, 2000; *Mignot et al.*, 2006; *Skinner et al.*, 2015). The application of these models has allowed the mapping of regions at risk of inundation from coastal (e.g. *Westerink et al.*, 1992; *Poulter and Halpin*, 2008; *Lewis et al.*, 2013; *Quinn et al.*, 2013; *Skinner et al.*, 2015; *Ramirez et al.*, 2016), fluvial (*Bates et al.*, 1992; *Werner et al.*, 2005; *Mignot et al.*, 2006; *Yu and Lane*, 2006; *McMillan and Brasington*, 2007; *Tayefi et al.*, 2007; *Wilson et al.*, 2007; *Apel et al.*, 2009; *Falter et al.*, 2013; *Yin et al.*, 2013; *Rudorff et al.*, 2014; *Jung and Merwade*, 2015) and pluvial (e.g. *Chen et al.*, 2005; *Schubert et al.*, 2008; *Leandro et al.*, 2009; *Sampson et al.*, 2012; *Liu et al.*, 2015; *Yu and Coulthard*, 2015) flood

events. However, flood inundation models are approximations of reality and are therefore subject to a number of uncertainties. These uncertainties include aleatory uncertainties relating to the randomness of a flood event occurring in the first place and epistemic uncertainties which exist as a result of our inexact understanding of the environment being modelled, such as uncertainties in the model structure (for example the underlying equations and numerical methods), parameters and boundary conditions (*Merz and Thieken*, 2005; *Renard et al.*, 2010; *Warmink et al.*, 2010; *Beven et al.*, 2011). In hydraulic modelling, many studies have looked at the effect of these uncertainties on predictions of flood hazards (*Romanowicz and Beven*, 1997; *Apel et al.*, 2004; *Hall et al.*, 2005; *Pappenberger et al.*, 2005; *Pappenberger et al.*, 2006; *Apel et al.*, 2008; *Di Baldassarre and Montanari*, 2009; *Domeneghetti et al.*, 2013). These uncertainties are typically represented probabilistically by computing multiple realisations of the model under different forcing conditions informed by the uncertainties under consideration, for example using the Generalised Likelihood Uncertainty Estimation (GLUE) methodology (*Beven and Binley*, 1992). The resultant suite of simulations may contain multiple models that satisfy the performance criteria set when assessing the skill of the models, a phenomenon often referred to as equifinality (*Beven and Freer*, 2001; *Savenije*, 2001; *Beven*, 2006; *Ebel and Loague*, 2006; *Vrugt et al.*, 2009).

An important decision faced by flood inundation modellers is the representation of topography. Advances in remote sensing over the last two decades have increased the availability of high resolution elevation data that can be utilised to represent topography by modellers, particularly through the increase in abundance of data collected through Light Detection and Ranging (LIDAR) imagery (i.e. *Bates*, 2012). These data are valuable for flood inundation models as finer resolution topography will allow smaller floodplain features to be explicitly represented within the Digital Elevation Model (DEM). The combination of high

resolution LiDAR data with computational advances and improved coding, for example, running simulations on Graphical Processing Units (GPUs) (*Lamb et al.*, 2009; *Kalyanapu et al.*, 2011) and parallelised model codes (*Neal et al.*, 2009; *Yu*, 2010) has enabled hydraulic models to simulate flood events at resolutions fine enough to resolve urban areas where buildings and roads have a major control on the inundation patterns observed (*Werner et al.*, 2005; *Yu and Lane*, 2006; *Fewtrell et al.*, 2008; *Neal et al.*, 2011; *Parkes et al.*, 2013; *Sampson et al.*, 2014). However, running multiple models at such fine scale resolutions remains computationally expensive, which limits our ability to fully analyse the inherent uncertainties of the modelling process by running multiple model realisations. Consequently, topographic data is commonly resampled to a coarser resolution than its original form, however the choice of method applied to produce the coarser DEM can result in different model predictions (*Fewtrell et al.*, 2008).

The development of more spatially complex models opens up a complexity-uncertainty trade off, whereby for a given amount of computational resource the total number of Monte Carlo simulations that can be run to quantify uncertainty in model predictions is limited by the spatial complexity of the model. One example of this issue is described by *Beven et al.* (2015) where the requirement for multiple simulations for forecast ensembles competes with the increasing spatial complexity of models. Despite the increasing availability of high quality data, the continued improvement in hydraulic models and computational advances, one of the key barriers for a more widespread uptake of flood inundation models for decision making during emergency situations is the time taken to perform simulations (*Leskens et al.*, 2014). This time is highly dependent on the spatial resolution of the model, particularly for models developed on Cartesian grids where the simulation run time increases by approximately an order of magnitude for a doubling of resolution (*Bates et al.*, 2010). Furthermore, the choice

of spatial resolution is subjective like many other choices made in the modelling process (*Pappenberger et al.*, 2007b), yet it could have key implications on the output of flood inundation models. It is therefore important to understand the relative importance of spatial resolution in comparison to other uncertainties, particularly if a model will be utilised to inform time critical decisions.

A formal methodology that allows us to explore the complexity-uncertainty trade-off is Sensitivity Analysis (SA). SA quantifies the contribution of various input factors, e.g. the model's forcing data, parameters or boundary conditions, to the variability in the model output (*Saltelli et al.*, 2008). SA techniques are typically classified into two main groups, local and global strategies. Local methods vary uncertain input factors in the neighbourhood of a nominal value, for instance the "optimal" parameter estimate. Global Sensitivity Analysis (GSA) strategies instead vary the input factors across a wider pre-defined region that reflect the modeller's estimate of the uncertainty in each factor (*Saltelli et al.*, 2008; *Pianosi et al.*, 2016). Furthermore, global methods such as the Sobol' method (*Sobol*, 2001) allow all factors to be varied simultaneously, so that interactions among input factors can be evaluated. In recent years the use of GSA has become feasible for increasingly complex environmental models (*van Werkhoven et al.*, 2008; *Nossent et al.*, 2011; *Yang*, 2011; *Zhang et al.*, 2013; *Hartmann et al.*, 2015). In hydraulic modelling, GSA has been utilised to understand the dominant processes affecting model performance (*Bates and Anderson*, 1996), for defence breach (*de Moel et al.*, 2012) and dam break scenarios (*Hall et al.*, 2009), to assess how influence of channel friction parameter varied downstream (*Hall et al.*, 2005) and to understand how implied sensitivities vary when using different GSA methods (*Pappenberger et al.*, 2008).

Although we know that the choice of spatial resolution can have a large influence on hydraulic model output (*Bates et al.*, 1998; *Horritt and Bates*, 2001b; *Yu and Lane*, 2006; *Savage et al.*, 2016), only the studies by *Bates et al.* (1998) and *Savage et al.* (2016) have considered this effect alongside other inherent uncertainties and none have done so using a formalised sensitivity analysis framework. In this paper we close this gap and demonstrate the use of GSA to quantify the relative importance of the choice of spatial resolution and the uncertainty this introduces when resampling a DEM in comparison to uncertainties in the boundary conditions and model parameters for flood inundation predictions. We use the hydraulic model LISFLOOD-FP (*Bates and De Roo*, 2000; *Bates et al.*, 2010) and Sobol's variance-based GSA method (*Saltelli et al.*, 2008). Using variance-based GSA allows us to incorporate both continuous variables such as model parameters and discrete choices like the spatial resolution of the model, using a tailored sampling strategy similar to the one adopted by *Baroni and Tarantola* (2014). By applying such a methodology we show how GSA can be applied to complex, spatially-distributed models using input factors that extend beyond the commonly incorporated model parameters and boundary conditions. This approach is transferrable to other environmental models for example in cases where modellers are interested in understanding the importance of decisions during model set-up in comparison to other uncertainties. We analyse different spatially and temporally variable flood outputs including flood extent, water depth and floodwave travel time. This allows us to explore whether model sensitivities to different input factors change in time and space and how implied sensitivities differ depending on the flood output assessed. By analysing the importance of spatial resolution in relation to other uncertain input factors, our approach also allows us to explore whether it would be more beneficial to spend computational resources running fewer models at finer spatial resolutions or running an increased number of simulations that explore the effect of other uncertain factors at coarser spatial resolutions.

2. Methodology

Figure 1 summarises the methodology applied in this study, which comprises four steps: the definition of the variability space of the input factors (Step 0 in Figure 1); the definition of which input factor combinations will be sampled (Step 1); the execution of the model (Step 2); and finally the quantification of the relative influence of the input factors on output variability by means of sensitivity indices (Step 3). In the following paragraphs we will provide more details on the key elements used at each of these steps, including the hydraulic model and the study site area (Sec. 2.1 and 2.2.), the definition of the sensitivity indices (Sec. 2.3), the sampling approach (Sec. 2.4), the definition of the variability space of the input factors (Sec. 2.5) and the choice of model outputs to be analysed (Sec. 2.6).

2.1 Case Study

The case study area used in this application is the Imera basin in Sicily which covers an area of approximately 2000 km^2 (*Aronica et al.*, 1998). The river flows southwards from the centre of Sicily to the coastal city of Licata where it meets the Mediterranean Sea. The floodplain is mostly rural with land mainly used for agricultural purposes. There are artificial levees along the major roads on the floodplain with flood defences located in the urban development of Licata. There is also a venturi-flume structure in the Imera channel upstream of Licata that partially restricts the flow during flood events and diverts some of the flow along a secondary channel. This meant that the Southern region of the basin was widely inundated on 12th October 1991 when 229 mm of rain fell at an intensity of up to 56 mm h^{-1} over a period of 21 hours (*Aronica et al.*, 1998). Data available to model this flood event using a flood inundation model include a 2 m Digital Elevation Model (DEM) covering an area of 50 km^2 and collected from LiDAR (see *Savage et al.*, 2016, Figure 1) with a vertical accuracy of ± 0.3 m,

and a hydrograph of the flood event that has been reconstructed through rainfall-runoff modelling and has been used previously by *Aronica et al.* (2002). The hydrograph had to be reproduced as the river gauge was washed away during the flood. Observational data of the flood exists in the form of heights of water marks collected at 25 locations and an outline of the flood extent collected post-event using loss data and field surveys. Previous studies have already demonstrated the ability of hydraulic models to simulate the observed flooding reasonably well for this event in comparison to these observational data (*Aronica et al.*, 2002; *Savage et al.*, 2016) so our analysis will focus on model predictions and behaviours rather than on performance against observed data.

2.2 Hydraulic Model

The hydraulic model used in this study is LISFLOOD-FP (*Bates and De Roo*, 2000; *Bates et al.*, 2010). This is an explicit finite difference model that solves an inertial approximation of the shallow water equations where advection is neglected. The equation used to calculate flow between two cells is:

$$Q^{t+\Delta t} = \frac{q^t - g h_{flow}^t \Delta t \frac{\Delta(h^t + z)}{\Delta x}}{(1 + g\Delta t n^2 |q^t| / (h_{flow}^t)^{7/3})} \Delta x$$

Equation 1

Where Q is flow (m^3s^{-1}), g is acceleration due to gravity (ms^{-1}), h is depth (m), n is the Manning's coefficient of roughness ($sm^{1/3}$), q is water flux (m^2s^{-1}), t is time, Δx is cell resolution (m), z is cell elevation (m) and h_{flow}^t is the depth that water can flow through the lateral boundary of two adjoining grid cells (m), calculated as the difference between the highest bed elevation and the highest water surface elevation between two cells.

It is possible that applying inertial terms particularly at fine resolutions can lead to instabilities in the model solution (*Bates et al.*, 2010). To overcome this, (*de Almeida et al.*,

2012) introduced an additional diffusion term (θ) that adds a minor and controlled amount of diffusion, which has been shown to stabilise the model without significantly changing the results (*de Almeida and Bates*, 2013). We introduce this term for the finest spatial resolution in this study when Manning's friction coefficients are less than 0.03 as initial simulations found these simulations to otherwise be unstable.

This model has been proven to perform well in comparison to other hydraulic models for simulations of both rural and urban flood events and in comparison to analytical solutions (*Horritt and Bates*, 2001a; *Hunter et al.*, 2008; *Bates et al.*, 2010; *Néelz and Pender*, 2013). The version of the model applied will be the sub-grid channel implementation (*Neal et al.*, 2012). In this the channel is defined separately to the floodplain allowing the channel widths to be defined independently to the spatial resolution of the model. However, flows in both the channel and floodplain are coupled and solved using the same inertial Shallow Water Equation (SWE) approximation, as described by (*Neal et al.*, 2012). The channel width and bed elevations are extracted from the 2 m LiDAR data every 10 m along the channel. A mean of these values is taken at the coarsest resolution applied in this study (50 m), which then defines the channel geometry for all model simulations. The channel shape is fixed as rectangular for each model resolution. This approach allows the channel widths to remain fixed and consistent across the different spatial resolutions and DEMs, thus making them grid independent.

2.3 Variance-based Sensitivity Indices

The key idea of variance-based Sensitivity Analysis is to measure the relative influence of the uncertainty in each input factor by its contribution to the variance of the model output. In particular, for each input factor, two sensitivity indices are typically computed, the first-order sensitivity index (or main effect) and the total-order sensitivity (or total effect) (*Saltelli*,

2002). The former measures the direct contribution to the output variance from individual variations of a factor, while the latter measures the overall contribution both from individual variations and through interactions with other factors. High sensitivity indices indicate a large influence over the variability of the output whilst low sensitivity indices indicate a small influence. If the difference between the total and main effects is large then this indicates strong interactions with other input factors.

For each input factor, say the *i*-th, the two indices are defined as

$$S_i = V_{xi} [E_{\mathbf{x}_{\sim i}}(y|x_i)] / V(y)$$

Equation 2.1

$$ST_i = 1 - V_{\mathbf{x}_{\sim i}} [E_{xi}(y|\mathbf{x}_{\sim i})] / V(y)$$

Equation 2.2

where y is the (scalar) model output, x_i is the i-th input factor, $\mathbf{x}_{\sim i}$ is the vector of all input factors but the i-th (i.e. $\mathbf{x}_{\sim i} = [x_1,\ldots,x_{i-1},x_{i+1},\ldots x_M]$), E denotes the expected value and V the variance. In our case study, the model output *y* is a temporal or spatial aggregation of the simulation results produced by LISFLOOD-FP. The multiple definitions of *y* considered in this study will be described in Sec. 2.6. The five input factors that are assessed in this study are: (1) the spatial resolution of the model; (2) the Digital Elevation Model (DEM) that is obtained by resampling high resolution LiDAR data to coarser resolutions; (3) and (4) the model parameters (Manning's channel and floodplain friction coefficients); and (5) the boundary condition (the forcing hydrograph). Their space of variability and the strategy adopted to handle non-numerical input factors like the spatial resolution and the multiple realisations of the DEM generated by resampling fine resolution topographic data to coarser resolutions, are described in the next section

Given that the complexity of the relationship between input factors and the model response does not allow the sensitivity indices of Equations 2.1 and 2.2 to be computed analytically, we approximate their values using the estimators described in *Saltelli et al.* (2010). The uncertainty associated to these sensitivity estimates is assessed by bootstrapping (*Efron and Tibshirani*, 1993). In particular, we associate each estimated index with its mean, 5^{th} and 95^{th} percentile across a prescribed number of bootstrap resamples. Since confidence intervals defined by these percentiles might be too large to draw meaningful conclusions, we also use a different approach focusing on the input ranking provided by sensitivity estimates: for each bootstrap resample we derive the ranking of the input factors and then compute the proportion of bootstrap resamples where each input factor is ranked 1^{st}, 2^{nd}, 3^{rd}, 4^{th} and 5^{th} most influential. The consistency and values of these two approaches are discussed in the Results section. The sensitivity analyses were performed using the SAFE Toolbox (*Pianosi et al.*, 2015).

2.4 Sampling Strategy for Handling Numerical and Non-numerical Input Factors

In order to compute the sensitivity indices of Equations 2.1 and 2.2, all the input factors under study must be regarded as stochastic variables and are therefore associated with a probability distribution, from which input samples are drawn. This is not straightforward for input factors that are not immediately represented by numerical quantities, such as the spatial resolution of the model. . To handle such a situation where some input factors are represented by scalar numerical quantities while others are not, we use a sampling strategy similar to the one described in *Baroni and Tarantola* (2014) (earlier applications of such sampling approach are *Tarantola et al.* (2002) and *Lilburne and Tarantola* (2009)), and further illustrated in Figure 1.

First, each input factor is associated with a list of its possible realizations. It is important that the ranges or choices sampled are as indicative of the uncertainty or range of likely choices as possible. If one factor has a disproportionately large sampling range in comparison to other factors, then the computed sensitivity indices could be unfairly skewed towards this factor being identified as highly influential. For discrete variables like the spatial resolution, the list includes the finite number of possible choices for that input (for instance, a resolution of 10, 20, 30, 40 and 50 m in our application). For continuous variables like the model parameters, the list includes a very large sample of possible values so as to approximate the underlying continuous distribution (for instance, 100 values in the range [0.025-0.05] for the floodplain friction). Then, the index of each element in the list is defined as the desired scalar quantity x_i, and associated with a discrete uniform probability distribution. Following these definitions, sampling is performed with respect to the scalar indices x_1,..., x_M, while the model is evaluated against the original input factors defined by the sampled indices. Output samples so obtained are then used to approximate the main and total effects.

In our application, we use a list of 5 choices for the spatial resolution, 25 for the DEMs produced by resampling LiDAR data multiple times (and explained fully in Section 2.5.2), 100 for the forcing hydrograph, and 100 values for each of the two friction parameters, which corresponds to a total of 125,000,000 possible combinations of the forcing inputs. This is not an exhaustive list of possible input factors; other factors that could be assessed include the underlying equations and numerical methods of the hydraulic model and the uncertainty of the LiDAR data. However, our focus for this paper is on the influence of the spatial resolution and its comparative importance in relation to the manning's friction coefficient parameter, the inflow hydrograph and the resampling of elevation data to coarser DEMs, which are the input factors most commonly varied by studies undertaking uncertainty analysis or hydraulic model calibration (for example: *Aronica et al.*, 2002; *Werner et al.*,

2005; *Di Baldassarre and Montanari*, 2009; *Jung et al.*, 2012; *Domeneghetti et al.*, 2013). From this input variability space, we randomly draw a base sample of N=15,000 input combinations. Then the estimation of the main and total effects according to the approximation strategy described in *Saltelli et al.* (2010) requires the construction of an additional N/2 x M = 37,500 combinations of input factors, where M is the number of input factors, by recombining the elements in the base sample. In total, the model is thus evaluated against 52,500 input combinations.

2.5 Definition of variability space of the input factors

The following paragraphs provide details on the definition of the possible choices or range of variation of the five input factors.

2.5.1 Spatial Resolution

Here we consider five choices for the spatial resolutions: 10, 20, 30, 40 and 50 m. These values are chosen to encompass simulation run times ranging from seconds to minutes whilst also ensuring that the ability of the model to simulate the flood extent would remain consistent across all simulations. Previous studies that applied LISFLOOD-FP to this study site and other rural locations found the model to perform reasonably well at resolutions up to 50 m when comparing to flood observations (*Horritt and Bates*, 2001b; *Aronica et al.*, 2002; *Savage et al.*, 2016). Although models can be run at coarser spatial resolutions, these are typically for much larger regional scale domains encompassing many catchments (e.g. *Neal et al.*, 2012) and the model performance does tend to tail off even for rural floodplains. Conversely, models can also be run at finer resolutions, however given that the floodplain is predominantly rural, we felt that it was not necessary to resolve length scales finer than 10 m.

2.5.2 Digital Elevation Model

When running the hydraulic model at a coarser resolution, it is necessary to resample the fine scale LiDAR data to produce a coarser resolution DEM. Doing so inevitably leads to a loss of information regarding the sub-grid scale topographic variability. In order to understand how important this loss is for model predictions we produce 25 different DEMs for each spatial resolution and include the DEM choice among the input factors of our GSA.

These DEMs are produced by systematically sampling different elevation values within each of the coarser grid cells. This is achieved by splitting each of the coarser grid cells into 25 smaller cells (in a 5 x 5 matrix) and then extracting the ground elevations measured from LiDAR at the centre of each of these cells in turn. This gives 25 possible elevation values for each cell which are systematically chosen in order, producing 25 DEMs. We have chosen this approach as opposed to using a random sampling approach to ensure that the distance between each retained elevation value remains consistent with the spatial resolution of the coarser DEM.

One limitation of this approach is that small scale features may not be represented in all of the resampled DEMs. Alternative methodologies that identify features within the coarser resolution DEMs, or other resampling approaches such as those investigated by (Fewtrell et al., 2008), could be adopted by other modellers to allow small-scale features to be represented in coarser DEMs. These approaches typically aim to produce the best representation of topography, however when resampling a DEM to a coarser resolution there are a number of possible nodal elevation values that could be retained in the new DEM and it is the variation in the underlying topography that we are exploring in this paper.

2.5.3 Manning's Friction Coefficients

The parameter most commonly calibrated in hydraulic modelling studies and therefore the parameter that is varied within our GSA is the Manning's roughness coefficient. We take the

353 approach chosen by many hydraulic modelling studies (i.e. *Horritt and Bates*, 2001a; *Aronica*
354 *et al.*, 2002; *Werner et al.*, 2005; *Jung et al.*, 2012) where the Manning's coefficient is
355 spatially disaggregated into two values only, one for the floodplain and the other for the
356 channel. This approach is broadly justified by Werner *et al.* (2005) who found that there is
357 little benefit in applying spatially distributed roughness parameters. When the uncertainty of
358 these parameters is considered in modelling studies, these parameters are typically sampled
359 from a wide parameter space with sampled values often outside the physically realistic range
360 for their environment (e.g. *Pappenberger et al.*, 2007a). This reflects that parameters are
361 often treated as effective parameters which subsume many of the other errors in the
362 modelling process. However if the parameter sample space is unrealistically large then the
363 sensitivity indices of these parameters may increase inappropriately (e.g. *Kelleher et al.*,
364 2013). Therefore in this study we assess the plausible space from which to sample these
365 parameters by comparing images of the Imera channel and surrounding floodplain with
366 Manning's friction definitions in the literature (*Chow*, 1959; *Arcement and Schneider*, 1989).
367 The plausible ranges for the roughness parameters are subsequently chosen as 0.025 – 0.04
368 for the channel and 0.025 – 0.05 for the floodplain. A total of 100 roughness coefficients
369 were sampled for each parameter within those ranges.

370 **2.5.4 Boundary Conditions**

371 The lack of gauged data for this flood event means that we are unable to make a more
372 informed assessment of the specific discharge uncertainty characteristics, for example by
373 performing a rating curve analysis (*Di Baldassarre and Montanari*, 2009; *McMillan et al.*,
374 2012; *Coxon et al.*, 2015). Instead, as the base hydrograph was recreated through rainfall
375 runoff modelling (*Aronica et al.*, 1998), we represent the boundary condition uncertainty by
376 applying an additive residual model to represent the fact that errors from rainfall runoff
377 models typically show signs of autocorrelation and heteroscedasticity (*Schoups and Vrugt*,

2010; *Pianosi and Raso*, 2012). This error model is easily transferrable to other time series data where it is known that the data may be subject to error. The method requires two parameters to be defined, the α-parameter and the β-parameter. These parameters control the proportion of error that propagates into the next timestep and the amount of error respectively. This reflects that errors are unlikely to change erratically during a singular event.

The perturbed discharge $Q_{updated}$ at a given timestep t is calculated as the base discharge Q_{base} multiplied by the residual error term ρ:

$$Q_t^{updated} = Q_t^{base} + \rho_t$$

Equation 2.3

Where the residual error term ρ is a function of the α-parameter, the error term at the previous time step and the discharge error term ε:

$$\rho_t = \alpha\rho_{t-1} + \varepsilon_t$$

Equation 2.4

The discharge error term ε can take both positive and negative values and is randomly sampled from a normal distribution between the values zero and the fractional error term σ:

$$\varepsilon_t \sim N([0, \sigma_t])$$

Equation 2.5

Where σ is a function of the β-parameter and Q_{base}:

399 $$\sigma_t = \beta Q_t^{base}$$

400 Equation 2.6

401 This set of equations is computed for each timestep to calculate a perturbed hydrograph that
402 is then used as a potential boundary condition.

403 When applying this error model, the parameters are set to control the amount and propagation
404 of error introduced to the timeseries data. Like the Manning's friction parameters, the values
405 applied to these parameters are critical in determining the variability within the perturbed
406 time series data generated and subsequently the calculation of sensitivity indices. The
407 assumption of normal errors combined with the properties of variance and application of a
408 Gaussian distribution allows Equations 2.4 and 2.6 to be reformulated to determine the value
409 at which three standard deviations of the residuals will fall between, shown in Equation 2.7:

410 $$\rho_{3SD} = \pm \frac{3\beta}{\sqrt{1 - \alpha^2}}$$

411 Equation 2.7

412 Discharge uncertainty for gauged flows has previously been estimated to be up to 40 % (*Di*
413 *Baldassarre and Montanari*, 2009; *McMillan et al.*, 2012) and we may expect this to be at the
414 upper limits in this case where the discharge has been reproduced using a rainfall-runoff
415 model rather than measured (*Aronica et al.*, 1998) and where the flooding experienced was an
416 extreme event. We have therefore set our parameter values to allow approximately three
417 standard deviations of the error residuals to be within 40 % of the base discharge level. This
418 amount of uncertainty is consistent with higher estimates of boundary condition uncertainty
419 and reflects the use of a reconstructed hydrograph and the extremity of the event. To allow
420 for these error characteristics we assign the α-parameter a value of 0.3 and the β-parameter a
421 value of 0.127. The error model is then run 100 times to produce 100 different perturbed

boundary condition realisations, which are shown within Figure 1. It is important to note that there are many ways that hydrograph uncertainty can be assessed and different parameter combinations could be applied. However the spread of uncertainty in the perturbed hydrographs appears sensible (Figure 1) and we therefore believe our method to be adequate to meet the objectives of this study.

2.6 Definition of Model Outputs

Previous studies using LISFLOOD-FP at this location have shown that the model is able to perform reasonably well when compared to observed data (*Aronica et al.*, 2002; *Savage et al.*, 2016). This allows us to assess a number of other model predictions at a temporal and spatial resolution that is far greater than any currently available datasets, enabling us to develop an understanding on how model sensitivities vary through time and space.

We assess both spatially lumped and spatially distributed model outputs. The spatially lumped variables that we assess our model simulations against are the Average Maximum Water Depth (AMWD) across the domain, calculated by taking the average of the maximum water depth across all cells that experienced flooding, and the maximum flood extent, defined as the percentage of cells flooded (where maximum water depth is greater than 0.10 m) in the domain. Since both of these variables vary along the simulation horizon, we introduce a temporal disaggregation. Model output is therefore assessed at 11 time slices to represent different stages of the flood event. We also define spatially disaggregated outputs by taking a grid of locations with an interval of 500 m. At each of these locations we consider as model outputs the time of initial and maximum inundation and the maximum water depth over the simulation horizon. Additionally we assess the spatial sensitivity of water depth to the different input factors at each of the 11 time slices. This combination of outputs allows us to capture whether model sensitivities vary spatially and temporally during a flood event.

3. Results

3.1 Spatially Lumped Outputs

Figure 2 reports the first-order sensitivity indices (Equation 2.1) for the maximum flood extent and Average Maximum Water Depth (AMWD). We can see from the top panels of Figure 2 that the values of the sensitivity indices are highly variable when computed over different bootstrap resamples. This indicates that the sample size is too small for the sensitivity indices to be estimated precisely. However, *Sarrazin et al.* (2016) have shown that precision and convergence of GSA results is reached at different sample sizes depending on the GSA aspect being assessed, e.g. the value of the sensitivity indices or the ranking of the input factors based on those values. This is relevant for this study as we are interested primarily in determining the most influential input factors rather than the exact values of the sensitivity indices. The bottom panels of Figure 2 show the rankings of input factors based on the sensitivity indices obtained at different bootstrap resamples. Each input factor takes a specific position in such rankings with a clearly highest frequency: for example in the bottom left panel, hydrograph (Hyd) is most often ranked first, flood friction (Flo) second, channel friction (Cha) third, spatial resolution (Res) fourth, and DEM fifth. Notice that this ranking is also consistent with the ranking of the mean value of sensitivity indices shown in the top left panel. We therefore consider the ranking of factors sufficiently precise and from now on will use look at rankings rather than the values of the sensitivity indices themselves.

From Figure 2 we can identify that the boundary conditions are the most influential factor for both outputs. The channel and floodplain friction parameters were the second most influential factors for maximum flood extent and AMWD respectively.

The fact that the boundary conditions are influential for maximum flood extent and AMWD is intuitive as the volume of water that enters the basin directly influences the volume of

water available to inundate the floodplain especially for a large flood event where out of bank flow is inevitable. It is also intuitive for the channel friction to be influential for flood extent as a higher Manning's friction coefficient will increase the frictional force of water in the channel, reducing its velocity and consequently increasing the channel water level so that more water would flow out of bank. Likewise the influential effect of the floodplain friction parameter for AMWD would be similar, by having a larger frictional force the velocity of flood waters on the floodplain is reduced, which allows water to build up; increasing water depths. The effect of the spatial resolution and DEM resampling is shown to be relatively unimportant for these outputs, meaning that any variations on a local scale are cancelled out when averaged out over the whole domain indicating that there are no large scale variations in conveyance between the different resolutions and DEMs.

When assessing how flood extent varies over the simulation horizon we see that the most influential input factor changes in time (Figure 3). The middle panel in this Figure reports the proportion of bootstrap resamples where an input factor was ranked most influential at a time slice. It shows that the factor that has the most influence on flood extent at the start of the flood is the boundary condition, however as the flood extent increases, the channel friction parameter becomes the most influential factor. This remains the case until the flood wave is almost fully receded at which point the floodplain friction parameter becomes the most influential factor. Although we might expect locally high floodplain velocities close to the channel as the floodplain drains, the fact that floodplain friction becomes influential at the end of the event for the spatially aggregated flood extent is unexpected given the small velocities experienced on the majority of floodplain and the resulting small frictional force. However at this stage in the simulation the incoming discharge is small meaning there is little absolute variation in the perturbed hydrographs. Consequently the effect of the channel friction parameter is also reduced as the river velocities will be decreased while frictional

495 force is proportional to Manning's friction parameter and the square of velocity. This
496 illustrates that during the drying phase of a flood event, which could be important for
497 assessments regarding how long a location is inundated for, it is important to account for
498 uncertainty in the floodplain friction parameter. However uncertainty in the input factors
499 produces less variation in flood extent at the end of the simulation than during the flood peak.

500 Interestingly, although the boundary conditions are most influential for maximum flood
501 extent (Figure 2), the channel friction is ranked the most influential for the majority of time
502 slices (middle panel in Figure 3). This is because once bankfull discharge is reached, the
503 channel friction parameter has the most influence on how quickly water is routed onto the
504 floodplain and therefore affects the rate of floodplain inundation, whereas the boundary
505 conditions are more influential on the maximum limit that floods will spread to within the
506 domain and how quickly bankfull discharge is reached as these are controlled by the volume
507 of water available to flood. The fact that the influence of Manning's roughness coefficients
508 changes during a flood event indicates that it may be important for future studies to allow
509 these parameters to be either time or depth varying parameters.

510

511 The bottom panel of Figure 3 reports the difference between the total-order sensitivity index
512 (Equation 2.2) and the first-order sensitivity index (Equation 2.1), averaged over all bootstrap
513 resamples. Such differences give an indication of the degree of interaction of each input
514 factor with the others. Results in the bottom panel show that interactions among input factors
515 are minimal during the wetting phase of the flood event but increase as the flood wave starts
516 to recede. Interestingly, the spatial resolution of the model and, particularly towards the end
517 of the simulation, the choice of DEM show high levels of interactions. Variations in the
518 topography caused by the different spatial resolutions and DEMs could lead to different

519 floodplain flow pathways that would be blocked or opened up depending on the sampling of
520 these factors. This suggests that during the wetting phase where there is minimal interaction,
521 the water levels are sufficiently large to overcome any potential blockages or flow pathways
522 because of the extensive overland flow. However at the end of the flood event, the channel
523 water levels drop and water is supra-elevated on the floodplain above the hydraulic gradient.
524 This water then finds its way back to the channel along smaller pathways than during the
525 wetting phase. Consequently, variations in these smaller pathways caused by differences in
526 the spatial resolution and sampling of the DEM exert most influence on the draining of the
527 water on the floodplain back to the channel. This reflects a change in the dynamics of the
528 flood event as the rising limb is usually much shorter than the falling limb and this affects the
529 ability to identify the operation of smaller pathways during the wetting phase. This hysteresis
530 behaviour has previously been identified in the field (*Nicholas and Mitchell*, 2003) and in
531 both rural (*Bates et al.*, 2006) and urban (*Neal et al.*, 2011) flood inundation modelling
532 studies.

533 **3.2 Spatially Distributed Outputs**

534 The top panel of Figure 4 reports sensitivity of maximum water depth at different locations in
535 the model domain. It shows that there is large spatial variability in the classification of the
536 most influential input factor. Although spatial resolution and choice of DEM are not highly
537 influential when water depths are averaged over the whole domain (Figure 2), we find these
538 factors to be more influential in many areas when assessing individual locations. The spatial
539 resolution of the model is most commonly ranked as the most influential factor across the
540 basin. One reason for this could be a result of differences in the representation of floodplain
541 features and embankments at different spatial resolutions. Furthermore, an extreme difference
542 in the elevation between neighbouring cells could alter flow pathways that would
543 significantly affect local inundation patterns. Over the whole domain, however, this effect is

544 averaged out across the cells, which is why we do not see similar influence of spatial
545 resolution for the spatially lumped outputs. This shows that if a decision maker is concerned
546 with water depths at a specific location then the spatial resolution and DEM becomes very
547 important. However despite this, there are still locations in the flood domain where the
548 influence of parametric and boundary condition uncertainty overcomes the local surface
549 elevation variability introduced by the choice of spatial resolution and the resampling of the
550 DEM.

551 Figure 5 shows how these sensitivities vary over time at each of the 11 time slices during the
552 flood event. From this Figure it can be seen that there is significant spatial and temporal
553 variability in identifying the most influential input factor across the basin. The general pattern
554 we see is that the hydrograph appears to be most influential factor at a location first, followed
555 by channel friction and then spatial resolution. Finally the choice of DEM becomes highly
556 influential during the drying phase. The floodplain friction parameter appears to be the least
557 influential and does not become influential during the drying phase unlike for flood extent.
558 This can be explained as the water depth of a cell does not explicitly consider those cells that
559 are classified as dry, while the flood extent does. Furthermore, a location may only remain
560 inundated due to certain elevations for certain DEMs, whereas the effect of individual cells
561 would be averaged out at the domain level that the flood extent is calculated for. This
562 highlights an advantage of assessing both temporally and spatially lumped and distributed
563 outputs as it allows different model dependencies and sensitivities to be identified.

564 **3.3 Time of Inundation**

565 The bottom panel of Figure 4 indicates that there are also spatial variations of the sensitivity
566 of the initial and maximum inundation timings. As with water depth, there is significant
567 spatial variability in determining the most influential input factor. The factor most influential

for the time of initial inundation is not necessarily the same as the factor most influential for the time of maximum inundation. The most influential factor for the eastern part of the flood basin remains the same for both and there is a large section of the NE basin that is highly sensitive to the channel friction parameter for both indicators. There is a region in the centre of the basin (2422879, 4109638) that is most sensitive to the channel parameter for the time of initial inundation, but becomes sensitive to the boundary conditions for the time of maximum inundation. One reason for this could be the fact that in some of the hydrograph perturbations the maximum discharge is reached one hour earlier than for others (Figure 1). Any location that is influenced by spatial resolution or the DEM for one output is likely to be influenced by the same factor for the other output. This indicates that the pattern of surface elevation is having a significant effect on the routing of flood waters to these locations.

4. Discussion

Incorporating spatial resolution into a Global Sensitivity Analysis of a flood inundation model has allowed us to gain new insights into how the sensitivities of different flood inundation model outputs vary in both time and space. By identifying the outputs for which different input factors become influential we can highlight, depending on the output of interest, how these factors may benefit from further knowledge/observations, research and development. This would help us to improve future model predictions through enhancements in the quality of data (if improving the boundary conditions, model parameters and DEM).

As discussed in Section 3.1, it became apparent early in the analysis that the sample size was too small for the convergence of the sensitivity indices to be reached. However we found that, despite the uncertainties in the sensitivity index values, the ranking of input factors was robust and consistent with the ranking obtained by considering the mean of the sensitivity

indices over the bootstrap resamples. This is shown particularly in Figures 3, 4 and 5 where on many occasions the proportion of bootstraps where a specific factor is ranked most influential was close to 100%. The fact that the ranking of factors is robust even if the values of the indices themselves were still very uncertain is not surprising and is consistent with previous findings (e.g. *Sarrazin et al.*, 2016).

We have ascertained that the factors identified as most influential vary depending on the chosen model output. This agrees with a previous study by *Pappenberger et al.* (2008) who found that different factors were influential for different performance metrics. It is therefore not possible to identify singular factors that are consistently influential across all outputs. Given the complex nonlinearities of simulating a flood using an inundation model and the relatively intuitive importance of the different input factors considered in this study this is perhaps not surprising. This result also suggests that the sampling strategy has not biased the computed sensitivity indices by over or under exaggerating our input factor sampling ranges. That is, none of the input factors have been classified as influential (or not) due to unreasonably large (or small) bounds in the sampling range. In other cases where the number of parameters is much larger it may be that a subset of influential factors is identified more easily (e.g. *Dobler and Pappenberger*, 2013).

We have shown that using lumped outputs alone may hide temporal and spatial variability in factor influence. Particularly interesting findings include the differences in the classification of influential factors between spatially lumped and distributed predictions of water depth and the changing sensitivity of the model when assessing changes in flood extent during a flood simulation.

Although we have shown that the model sensitivities vary across space, time and chosen output, our findings indicate that some of the input factors may require more or less

consideration depending on the decisions that the flood inundation model is being used to support. If a decision maker requires predictions of maximum flood extent, for example when producing return interval flood hazard maps (i.e. *Neal et al.*, 2013), our particular case study analysis suggests that it would be most important to consider the boundary conditions and the Manning's channel friction parameter. This partly agrees with *Hall et al.* (2005) who found that the Manning's channel friction parameter was the most influential factor when assessing flood extent against observational data. Despite this we would expect that the most influential factor for different model outputs could vary depending on the specific characteristics of the study site chosen, the quality of the input data, the model structure and the sampling approach adopted to consider uncertainties in the model parameters and boundary conditions.

We also assessed the sensitivity of flood extent through time, which has not been evaluated previously. The variation in the most influential factor through time, from the boundary conditions to the channel friction and finally to floodplain friction, indicates that if a decision maker is interested in the dynamics of inundation through the passage of the flood wave then they should carefully consider each of these uncertainties. It is important to note that the variation in modelled flood extent at the end of the flood event is smaller than the variation during the peak of the flood (Figure 3). However, the influence of floodplain friction on the recession of floodwaters could still be of interest for emergency planners who may be concerned with quantifying the uncertainty when determining how quickly flood waters will recede, for example for traffic management if roads or railways become inundated. Furthermore, the recession and duration of a flood event is also of interest for insurance purposes, such as for estimating business interruption losses, though the importance of floodplain friction would depend on the uncertainty of the boundary conditions for a given forecast or design flood event.

It is clear for an event of this magnitude that when determining flood extent, spatial resolution and DEM are not influential on their own. However the fact that they show signs of interaction with other factors as flood waters recede suggests that the different topographic realisations do exert an influence on the flow paths flood waters take when draining from the floodplain. As this was a large flood event where the rising limb was much more rapid than the falling limb, it is perhaps not surprising that spatial resolution and the DEM were not influential during the wetting phase of the event as the floodwaters would be deep enough to traverse the small scale fluctuations in topography caused by changing spatial resolution and DEM. However, for a smaller flood this may not be the case if the floodwaters are much shallower. It would therefore be interesting to assess whether the sensitivity of flood extent changes for different magnitude flood events and for events with different hydrological characteristics.

The choice of spatial resolution and DEM does become important for local scale predictions of water depth, but not at the expense of parameter and boundary condition uncertainty. The spatial and temporal variability of the models' sensitivity to each these factors (except for floodplain friction) reflects the complexity of predicting water depths and suggests that a finer model resolution may be necessary if a decision maker is interested in local scale inundation predictions. The variability of water depth sensitivity is consistent with the findings by *Pappenberger et al.* (2008) who also found boundary conditions and channel friction to be more influential than floodplain friction when comparing predictions of water depth against observational data. Modellers producing spatially distributed predictions of water depth should therefore carefully consider the resolution of their model and the uncertainty associated with degrading topographic data to coarser resolutions in their study, as for example assessed by *Fewtrell et al.* (2008). These spatial and temporal variabilities in output sensitivity to different input factors suggest that more complex observations of flood

events that vary in both time and space would be extremely valuable in benchmarking model performance and constraining behavioural model simulations.

Our analysis has therefore allowed us to identify that for some model applications, resources would be better spent on improving our understanding of the uncertain data, whilst for others it would also be important to improve the spatial resolution. The methodology we have applied in this study is transferable to other models where the modeller wishes to determine the relative influence of discrete choices and continuous variables within a Sensitivity Analysis. By including spatial resolution as a discrete variable, a modeller can use Sensitivity Analysis to assess whether running hyperresolution models (*Wood et al.*, 2011; *Beven et al.*, 2015) is really beneficial for their specific study example It would also be possible to apply a similar approach to assess the comparative influence of other discrete choices, such as the choice of hydraulic model or the adoption of time-varying Manning's friction coefficients. However it is important for future studies to carefully consider and document the definition of the variability space of input factors so as not to artificially influence the computed sensitivity indices. In fact, as also shown in other studies this definition can have a significant impact on the computed sensitivities, and therefore should be carefully considered when applying GSA. Any GSA study therefore only investigates a user specified region of the input factor space, which has to be defined by the modeller based on previous model applications or a priori information available. The GSA results are then conditional on the applied overall experimental design considering the assumptions and choices made.

Clearly there are limitations to extrapolating these findings to other flood events. These findings are valid for one model at one location and for a flood of one magnitude. The computed sensitivities and rankings of input factors may be different for different magnitude events and at different locations. For example for a smaller flood event where the channel bank-full level is only just reached, uncertainties in the boundary conditions and channel

friction parameters may be more important factors to include as they will determine whether or not rivers reach bank-full discharge. Alternatively, an urban environment where critical flow pathways get blocked at coarser resolutions may be more sensitive to the spatial resolution of the model. We also acknowledge that the ranking of input factors can also vary depending on the specific GSA method applied (*Pappenberger et al.*, 2008). However LISFLOOD-FP has been previously shown to perform similarly to a suite of other hydraulic models (*Hunter et al.*, 2008; *Néelz and Pender*, 2013) and similarities between our approach and those by *Hall et al.* (2005) and *Pappenberger et al.* (2008) are encouraging in terms of the applicability of the GSA approach undertaken in this study.

5. Conclusions

This study has applied a GSA methodology, which allowed us to assess whether variability in spatial resolution, DEM, model parameters or model boundary conditions produce the most variance in the output of the hydraulic model LISFLOOD-FP. For our case study we have found that the sensitivity to the various input factors changes in time and space and differs depending on the type of model output that is being assessed. For predictions of flood extent, the dominant input factor shifts during the flood event from the hydrograph to the channel friction and then to the floodplain friction. However, for localised water depths the spatial resolution and DEM become much more influential although there is a great deal of spatial and temporal variability as to which of the five factors is classified as most influential. We also found that the factors affecting the timing of flood waters at locations across the domain can be different to the factors that most influence water depths. It is therefore more important to account for the spatial resolution of a model for decisions based on water depths and time of inundation than for decisions based on the extent of a flood.

The fact that the sensitivities are so variable in time and space demonstrates the value that performing SA can add in gaining an understanding of these complex patterns and dependencies. It also demonstrates that a simple SA, in which spatial and temporal variability are ignored, can be very misleading. These complex behaviours are indicative of the non-linearity that is inherent in such flood events and demonstrate that it is not possible to identify a singular factor that is most influential for all types of flood inundation prediction.

Subsequent work should test whether output sensitivities differ for events of different magnitude and for events at different locations. Additionally, it would be useful to explore what impact the channel geometry has on the temporal and spatial variation in flood inundations and whether the observed variability in the sensitivity to water depths is also found when assessing predictions of velocity By improving our understanding of the factors that have the most influence on flood inundation predictions it will be possible to identify areas for future modelling improvements; whether that is a need for improved topographic representation, boundary condition data, parameter classification or model structures.

Finally, the approach adopted in this paper to include discrete, non-numerical choices within a GSA and to explore how sensitivity changes in time and space could be adopted by any modeller that wishes to learn more about the impacts of their choices and modelling assumptions on various aspects of the model's response.

6. Acknowledgements

The sources of hydrological data used as a baseline for this study are included in Section 2.1 and the authors would like to thank Giuseppe Aronica for providing these data. The LiDAR data used in this study can be obtained by contacting the Regione Siciliana – Assessorato del Territorio e dell'Ambiente – S.I.T.R. The SAFE toolbox is freely available for research purposes from www.safetoolbox.info. The authors would like to thank three anonymous

reviewers and Charles Luce for their insightful comments and suggestions, which helped improve this manuscript. This work was supported by the Natural Environment Research Council [Consortium on Risk in the Environment: Diagnostics, Integration, Benchmarking, Learning and Elicitation (CREDIBLE); grant number NE/J017450/1].

7. References

Apel H., B. Merz, A. H. Thieken. (2008), Quantification of uncertainties in flood risk assessments, *International Journal of River Basin Management*, *6*, 149-162, DOI: 10.1080/15715124.2008.9635344.

Apel H., B. Merz, A. H. Thieken. (2009), Influence of dike breaches on flood frequency estimation, *Comput Geosci-Uk*, *35*, 907-923, DOI: 10.1016/j.cageo.2007.11.003.

Apel H., A. H. Thieken, B. Merz, G. Bloschl. (2004), Flood risk assessment and associated uncertainty, *Nat Hazard Earth Sys*, *4*, 295-308.

Arcement G., V. Schneider. (1989), *Guide for Selecting Manning's Roughness Coefficients for Natural Channels and Flood Plains*, In: U.S. Geological Survey Water Supply Paper 2339, U. S. Government Printing Office.

Aronica G., B. Hankin, K. Beven. (1998), Uncertainty and equifinality in calibrating distributed roughness coefficients in a flood propagation model with limited data, *Adv Water Resour*, *22*, 349-365, DOI: Doi 10.1016/S0309-1708(98)00017-7.

Aronica G., P. D. Bates, M. S. Horritt. (2002), Assessing the uncertainty in distributed model predictions using observed binary pattern information within GLUE, *Hydrol Process*, *16*, 2001-2016, DOI: 10.1002/hyp.398.

Baroni G., S. Tarantola. (2014), A General Probabilistic Framework for uncertainty and global sensitivity analysis of deterministic models: A hydrological case study, *Environ Modell Softw*, *51*, 26-34, DOI: 10.1016/j.envsoft.2013.09.022.

Bates P. D. (2012), Integrating remote sensing data with flood inundation models: how far have we got?, *Hydrol Process*, *26*, 2515-2521, DOI: 10.1002/hyp.9374.

Bates P. D., M. G. Anderson. (1996), A preliminary investigation into the impact of initial conditions on flood inundation predictions using a time/space distributed sensitivity analysis, *Catena*, *26*, 115-134, DOI: Doi 10.1016/0341-8162(95)00041-0.

Bates P. D., A. P. J. De Roo. (2000), A simple raster-based model for flood inundation simulation, *J Hydrol*, *236*, 54-77, DOI: Doi 10.1016/S0022-1694(00)00278-X.

Bates P. D., M. Horritt, J. M. Hervouet. (1998), Investigating two-dimensional, finite element predictions of floodplain inundation using fractal generated topography, *Hydrol Process*, *12*, 1257-1277, DOI: Doi 10.1002/(Sici)1099-1085(19980630)12:8<1257::Aid-Hyp672>3.0.Co;2-P.

Bates P. D., M. S. Horritt, T. J. Fewtrell. (2010), A simple inertial formulation of the shallow water equations for efficient two-dimensional flood inundation modelling, *J Hydrol*, *387*, 33-45, DOI: 10.1016/j.jhydrol.2010.03.027.

Bates P. D., M. G. Anderson, L. Baird, D. E. Walling, D. Simm. (1992), Modelling floodplain flows using a two-dimensional finite element model, *Earth Surface Processes and Landforms*, *17*, 575-588, DOI: 10.1002/esp.3290170604.

Bates P. D., M. D. Wilson, M. S. Horritt, D. C. Mason, N. Holden, A. Currie. (2006), Reach scale floodplain inundation dynamics observed using airborne synthetic aperture radar imagery: Data analysis and modelling, *J Hydrol*, *328*, 306-318, DOI: 10.1016/j.jhydrol.2005.12.028.

Beven K. (2006), A manifesto for the equifinality thesis, *J Hydrol*, *320*, 18-36, DOI: 10.1016/j.jhydrol.2005.07.007.

Beven K., A. Binley. (1992), The Future of Distributed Models - Model Calibration and Uncertainty Prediction, *Hydrol Process*, *6*, 279-298, DOI: DOI 10.1002/hyp.3360060305.

786 Beven K., J. Freer. (2001), Equifinality, data assimilation, and uncertainty estimation in mechanistic
787 modelling of complex environmental systems using the GLUE methodology, *J Hydrol*, *249*,
788 11-29, DOI: Doi 10.1016/S0022-1694(01)00421-8.
789 Beven K., H. Cloke, F. Pappenberger, R. Lamb, N. Hunter. (2015), Hyperresolution information and
790 hyperresolution ignorance in modelling the hydrology of the land surface, *Sci China Earth*
791 *Sci*, *58*, 25-35, DOI: 10.1007/s11430-014-5003-4.
792 Beven K. J., D. T. Leedal, S. McCarthy, R. Lamb, M. Hunter, C. Keef, P. D. Bates, J. Neal, J. Wicks.
793 (2011), Framework for assessing uncertainty in fluvial flood risk mapping, *FRMRC Research*
794 *Report SWP1.7*.
795 Bradbrook K. F., S. N. Lane, S. G. Waller, P. D. Bates. (2004), Two dimensional diffusion wave
796 modelling of flood inundation using a simplified channel representation, *International*
797 *Journal of River Basin Management*, *2*, 211-223, DOI: 10.1080/15715124.2004.9635233.
798 Chen A. S., M. H. Hsu, T. S. Chen, T. J. Chang. (2005), An integrated inundation model for highly
799 developed urban areas, *Water Sci Technol*, *51*, 221-229.
800 Chow V. T. (1959), *Open-channel hydraulics*, McGraw-Hill.
801 Cook A., V. Merwade. (2009), Effect of topographic data, geometric configuration and modeling
802 approach on flood inundation mapping, *J Hydrol*, *377*, 131-142, DOI:
803 10.1016/j.jhydrol.2009.08.015.
804 Coxon G., J. Freer, I. K. Westerberg, T. Wagener, R. Woods, P. J. Smith. (2015), A novel framework
805 for discharge uncertainty quantification applied to 500 UK gauging stations, *Water Resour*
806 *Res*, n/a-n/a, DOI: 10.1002/2014WR016532.
807 de Almeida G. A. M., P. Bates. (2013), Applicability of the local inertial approximation of the shallow
808 water equations to flood modeling, *Water Resour Res*, *49*, 4833-4844, DOI:
809 10.1002/wrcr.20366.
810 de Almeida G. A. M., P. Bates, J. E. Freer, M. Souvignet. (2012), Improving the stability of a simple
811 formulation of the shallow water equations for 2-D flood modeling, *Water Resour Res*, *48*,
812 DOI: Artn W05528

813 10.1029/2011wr011570.
814 de Moel H., N. E. M. Asselman, J. C. J. H. Aerts. (2012), Uncertainty and sensitivity analysis of
815 coastal flood damage estimates in the west of the Netherlands, *Nat Hazard Earth Sys*, *12*,
816 1045-1058, DOI: 10.5194/nhess-12-1045-2012.
817 Di Baldassarre G., A. Montanari. (2009), Uncertainty in river discharge observations: a quantitative
818 analysis, *Hydrol Earth Syst Sc*, *13*, 913-921.
819 Dobler C., F. Pappenberger. (2013), Global sensitivity analyses for a complex hydrological model
820 applied in an Alpine watershed, *Hydrol Process*, *27*, 3922-3940, DOI: 10.1002/hyp.9520.
821 Domeneghetti A., S. Vorogushyn, A. Castellarin, B. Merz, A. Brath. (2013), Probabilistic flood
822 hazard mapping: effects of uncertain boundary conditions, *Hydrol Earth Syst Sc*, *17*, 3127-
823 3140, DOI: 10.5194/hess-17-3127-2013.
824 Ebel B. A., K. Loague. (2006), Physics-based hydrologic-response simulation: Seeing through the fog
825 of equifinality, *Hydrol Process*, *20*, 2887-2900, DOI: 10.1002/hyp.6388.
826 Efron B., R. J. Tibshirani. (1993), *An introduction to the bootstrap*, Chapman & Hall.
827 Falter D., S. Vorogushyn, J. Lhomme, H. Apel, B. Gouldby, B. Merz. (2013), Hydraulic model
828 evaluation for large-scale flood risk assessments, *Hydrol Process*, *27*, 1331-1340, DOI:
829 10.1002/hyp.9553.
830 Fewtrell T. J., P. D. Bates, M. Horritt, N. M. Hunter. (2008), Evaluating the effect of scale in flood
831 inundation modelling in urban environments, *Hydrol Process*, *22*, 5107-5118, DOI:
832 10.1002/hyp.7148.
833 Hall J. W., S. Tarantola, P. D. Bates, M. S. Horritt. (2005), Distributed sensitivity analysis of flood
834 inundation model calibration, *J Hydraul Eng-Asce*, *131*, 117-126, DOI: 10.1061/(Asce)0733-
835 9429(2005)131:2(117).
836 Hall J. W., S. A. Boyce, Y. L. Wang, R. J. Dawson, S. Tarantola, A. Saltelli. (2009), Sensitivity
837 Analysis for Hydraulic Models, *J Hydraul Eng-Asce*, *135*, 959-969, DOI:
838 10.1061/(Asce)Hy.1943-7900.0000098.

839 Hartmann A., T. Gleeson, R. Rosolem, F. Pianosi, Y. Wada, T. Wagener. (2015), A large-scale
840 simulation model to assess karstic groundwater recharge over Europe and the Mediterranean,
841 *Geosci Model Dev*, *8*, 1729-1746, DOI: 10.5194/gmd-8-1729-2015.
842 Horritt M. S., P. D. Bates. (2001a), Predicting floodplain inundation: raster-based modelling versus
843 the finite-element approach, *Hydrol Process*, *15*, 825-842, DOI: Doi 10.1002/Hyp.188.
844 Horritt M. S., P. D. Bates. (2001b), Effects of spatial resolution on a raster based model of flood flow,
845 *J Hydrol*, *253*, 239-249, DOI: Doi 10.1016/S0022-1694(01)00490-5.
846 Hunter N. M., P. D. Bates, S. Neelz, G. Pender, I. Villanueva, N. G. Wright, D. Liang, R. A. Falconer,
847 B. Lin, S. Waller, A. J. Crossley, D. C. Mason. (2008), Benchmarking 2D hydraulic models
848 for urban flooding, *P I Civil Eng-Wat M*, *161*, 13-30, DOI: 10.1680/wama.2008.161.1.13.
849 Jung H. C., M. Jasinski, J. W. Kim, C. K. Shum, P. Bates, J. Neal, H. Lee, D. Alsdorf. (2012),
850 Calibration of two-dimensional floodplain modeling in the central Atchafalaya Basin
851 Floodway System using SAR interferometry, *Water Resour Res*, *48*, DOI: Artn W07511

852 10.1029/2012wr011951.
853 Jung Y., V. Merwade. (2015), Estimation of uncertainty propagation in flood inundation mapping
854 using a 1-D hydraulic model, *Hydrol Process*, *29*, 624-640, DOI: 10.1002/hyp.10185.
855 Kalyanapu A. J., S. Shankar, E. R. Pardyjak, D. R. Judi, S. J. Burian. (2011), Assessment of GPU
856 computational enhancement to a 2D flood model, *Environ Modell Softw*, *26*, 1009-1016, DOI:
857 10.1016/j.envsoft.2011.02.014.
858 Kelleher C., T. Wagener, B. McGlynn, A. S. Ward, M. N. Gooseff, R. A. Payn. (2013), Identifiability
859 of transient storage model parameters along a mountain stream, *Water Resour Res*, *49*, 5290-
860 5306, DOI: 10.1002/wrcr.20413.
861 Lamb R., M. Crossley, S. Waller. (2009), A fast two-dimensional floodplain inundation model, *P I*
862 *Civil Eng-Wat M*, *162*, 363-370, DOI: 10.1680/wama.2009.162.6.363.
863 Leandro J., A. S. Chen, S. Djordjevic, D. A. Savic. (2009), Comparison of 1D/1D and 1D/2D Coupled
864 (Sewer/Surface) Hydraulic Models for Urban Flood Simulation, *J Hydraul Eng-Asce*, *135*,
865 495-504, DOI: 10.1061/(Asce)Hy.1943-7900.0000037.
866 Leskens J. G., M. Brugnach, A. Y. Hoekstra, W. Schuurmans. (2014), Why are decisions in flood
867 disaster management so poorly supported by information from flood models?, *Environ*
868 *Modell Softw*, *53*, 53-61, DOI: 10.1016/j.envsoft.2013.11.003.
869 Lewis M., P. Bates, K. Horsburgh, J. Neal, G. Schumann. (2013), A storm surge inundation model of
870 the northern Bay of Bengal using publicly available data, *Q J Roy Meteor Soc*, *139*, 358-369,
871 DOI: 10.1002/qj.2040.
872 Lilburne L., S. Tarantola. (2009), Sensitivity analysis of spatial models, *International Journal of*
873 *Geographical Information Science*, *23*, 151-168, DOI: Pii 902651821

874 10.1080/13658810802094995.
875 Liu L., Y. Liu, X. Wang, D. Yu, K. Liu, H. Huang, G. Hu. (2015), Developing an effective 2-D urban
876 flood inundation model for city emergency management based on cellular automata, *Nat*
877 *Hazard Earth Sys*, *15*, 381-391, DOI: 10.5194/nhess-15-381-2015.
878 McMillan H., T. Krueger, J. Freer. (2012), Benchmarking observational uncertainties for hydrology:
879 rainfall, river discharge and water quality, *Hydrol Process*, *26*, 4078-4111, DOI:
880 10.1002/hyp.9384.
881 McMillan H. K., J. Brasington. (2007), Reduced complexity strategies for modelling urban floodplain
882 inundation, *Geomorphology*, *90*, 226-243, DOI: 10.1016/j.geomorph.2006.10.031.
883 Merz B., A. H. Thieken. (2005), Separating natural and epistemic uncertainty in flood frequency
884 analysis, *J Hydrol*, *309*, 114-132, DOI: 10.1016/j.jhydrol.2004.11.015.
885 Mignot E., A. Paquier, S. Haider. (2006), Modeling floods in a dense urban area using 2D shallow
886 water equations, *J Hydrol*, *327*, 186-199, DOI: 10.1016/j.jhydrol.2005.11.026.
887 Neal J., T. Fewtrell, M. Trigg. (2009), Parallelisation of storage cell flood models using OpenMP,
888 *Environ Modell Softw*, *24*, 872-877, DOI: 10.1016/j.envsoft.2008.12.004.
889 Neal J., G. Schumann, P. Bates. (2012), A subgrid channel model for simulating river hydraulics and
890 floodplain inundation over large and data sparse areas, *Water Resour Res*, *48*, DOI: Artn
891 W11506

892 Doi 10.1029/2012wr012514.
893 Neal J., C. Keef, P. Bates, K. Beven, D. Leedal. (2013), Probabilistic flood risk mapping including
894 spatial dependence, *Hydrol Process*, *27*, 1349-1363, DOI: 10.1002/hyp.9572.
895 Neal J., G. Schumann, T. Fewtrell, M. Budimir, P. Bates, D. Mason. (2011), Evaluating a new
896 LISFLOOD-FP formulation with data from the summer 2007 floods in Tewkesbury, UK, *J*
897 *Flood Risk Manag*, *4*, 88-95, DOI: 10.1111/j.1753-318X.2011.01093.x.
898 Néelz S., G. Pender. (2013), *Benchmarking the latest generation of 2D hydraulic modelling packages*,
899 Environment Agency.
900 Nicholas A. P., C. A. Mitchell. (2003), Numerical simulation of overbank processes in
901 topographically complex floodplain environments, *Hydrol Process*, *17*, 727-746, DOI:
902 10.1002/hyp.1162.
903 Nossent J., P. Elsen, W. Bauwens. (2011), Sobol' sensitivity analysis of a complex environmental
904 model, *Environ Modell Softw*, *26*, 1515-1525, DOI: 10.1016/j.envsoft.2011.08.010.
905 Pappenberger F., K. Beven, M. Horritt, S. Blazkova. (2005), Uncertainty in the calibration of effective
906 roughness parameters in HEC-RAS using inundation and downstream level observations, *J*
907 *Hydrol*, *302*, 46-69, DOI: 10.1016/j.jhydrol.2004.06.036.
908 Pappenberger F., K. J. Beven, M. Ratto, P. Matgen. (2008), Multi-method global sensitivity analysis
909 of flood inundation models, *Adv Water Resour*, *31*, 1-14, DOI:
910 10.1016/j.advwatres.2007.04.009.
911 Pappenberger F., K. Frodsham, K. Beven, R. Romanowicz, P. Matgen. (2007a), Fuzzy set approach to
912 calibrating distributed flood inundation models using remote sensing observations, *Hydrol*
913 *Earth Syst Sc*, *11*, 739-752.
914 Pappenberger F., K. Beven, K. Frodsham, R. Romanowicz, P. Matgen. (2007b), Grasping the
915 unavoidable subjectivity in calibration of flood inundation models: A vulnerability weighted
916 approach, *J Hydrol*, *333*, 275-287, DOI: 10.1016/j.jhydrol.2006.08.017.
917 Pappenberger F., P. Matgen, K. J. Beven, J. B. Henry, L. Pfister, P. Fraipont de. (2006), Influence of
918 uncertain boundary conditions and model structure on flood inundation predictions, *Adv*
919 *Water Resour*, *29*, 1430-1449, DOI: 10.1016/j.advwatres.2005.11.012.
920 Parkes B. L., H. L. Cloke, F. Pappenberger, J. Neal, D. Demeritt. (2013), Reducing Inconsistencies in
921 Point Observations of Maximum Flood Inundation Level, *Earth Interact*, *17*, DOI: Artn 6

922 10.1175/2012ei000475.1.
923 Pianosi F., L. Raso. (2012), Dynamic modeling of predictive uncertainty by regression on absolute
924 errors, *Water Resour Res*, *48*, DOI: Artn W03516

925 10.1029/2011wr010603.
926 Pianosi F., F. Sarrazin, T. Wagener. (2015), A Matlab toolbox for Global Sensitivity Analysis,
927 *Environ Modell Softw*, *70*, 80-85, DOI: 10.1016/j.envsoft.2015.04.009.
928 Pianosi F., K. Beven, J. Freer, J. W. Hall, J. Rougier, D. B. Stephenson, T. Wagener. (2016),
929 Sensitivity analysis of environmental models: A systematic review with practical workflow,
930 *Environ Modell Softw*, *79*, 214-232, DOI: http://dx.doi.org/10.1016/j.envsoft.2016.02.008.
931 Poulter B., P. N. Halpin. (2008), Raster modelling of coastal flooding from sea-level rise,
932 *International Journal of Geographical Information Science*, *22*, 167-182, DOI:
933 10.1080/13658810701371858.
934 Quinn N., P. D. Bates, M. Siddall. (2013), The contribution to future flood risk in the Severn Estuary
935 from extreme sea level rise due to ice sheet mass loss, *J Geophys Res-Oceans*, *118*, 5887-
936 5898, DOI: 10.1002/jgrc.20412.
937 Ramirez J. A., M. Lichter, T. J. Coulthard, C. Skinner. (2016), Hyper-resolution mapping of regional
938 storm surge and tide flooding: comparison of static and dynamic models, *Nat Hazards*, 1-20,
939 DOI: 10.1007/s11069-016-2198-z.
940 Renard B., D. Kavetski, G. Kuczera, M. Thyer, S. W. Franks. (2010), Understanding predictive
941 uncertainty in hydrologic modeling: The challenge of identifying input and structural errors,
942 *Water Resour Res*, *46*, DOI: Artn W05521

943 10.1029/2009wr008328.

944 Romanowicz R., K. Beven. (1997), Dynamic real-time prediction of flood inundation probabilities,
945 *Hydrological Sciences Journal*, *43*, 181-196.
946 Rudorff C. M., J. M. Melack, P. D. Bates. (2014), Flooding dynamics on the lower Amazon
947 floodplain: 1. Hydraulic controls on water elevation, inundation extent, and river- floodplain
948 discharge, *Water Resour Res*, *50*, 619-634, DOI: 10.1002/2013wr014091.
949 Saltelli A. (2002), Making best use of model evaluations to compute sensitivity indices, *Comput Phys*
950 *Commun*, *145*, 280-297, DOI: Pii S0010-4655(02)00280-1

951 Doi 10.1016/S0010-4655(02)00280-1.
952 Saltelli A., P. Annoni, I. Azzini, F. Campolongo, M. Ratto, S. Tarantola. (2010), Variance based
953 sensitivity analysis of model output. Design and estimator for the total sensitivity index,
954 *Comput Phys Commun*, *181*, 259-270, DOI: 10.1016/j.cpc.2009.09.018.
955 Saltelli A., M. Ratto, T. Andres, F. Compolongo, J. Cariboni, D. Gatelli, M. Saisana, S. Tarantola.
956 (2008), *Global sensitivity analysis : the primer*, John Wiley.
957 Sampson C. C., T. J. Fewtrell, A. Duncan, K. Shaad, M. S. Horritt, P. D. Bates. (2012), Use of
958 terrestrial laser scanning data to drive decimetric resolution urban inundation models, *Adv*
959 *Water Resour*, *41*, 1-17, DOI: 10.1016/j.advwatres.2012.02.010.
960 Sampson C. C., T. J. Fewtrell, F. O'Loughlin, F. Pappenberger, P. B. Bates, J. E. Freer, H. L. Cloke.
961 (2014), The impact of uncertain precipitation data on insurance loss estimates using a flood
962 catastrophe model, *Hydrol Earth Syst Sc*, *18*, 2305-2324, DOI: 10.5194/hess-18-2305-2014.
963 Sarrazin F., F. Pianosi, T. Wagener. (2016), Global Sensitivity Analysis of environmental models:
964 Convergence and validation, *Environ Modell Softw*, *79*, 135-152, DOI:
965 http://dx.doi.org/10.1016/j.envsoft.2016.02.005.
966 Savage J. T. S., P. Bates, J. Freer, J. Neal, G. Aronica. (2016), When does spatial resolution become
967 spurious in probabilistic flood inundation predictions?, *Hydrol Process*, n/a-n/a, DOI:
968 10.1002/hyp.10749.
969 Savenije H. H. G. (2001), Equifinality, a blessing in disguise?, *Hydrol Process*, *15*, 2835-2838, DOI:
970 DOI 10.1002/hyp.494.
971 Schoups G., J. A. Vrugt. (2010), A formal likelihood function for parameter and predictive inference
972 of hydrologic models with correlated, heteroscedastic, and non-Gaussian errors, *Water Resour*
973 *Res*, *46*, DOI: Artn W10531

974 10.1029/2009wr008933.
975 Schubert J. E., B. F. Sanders, M. J. Smith, N. G. Wright. (2008), Unstructured mesh generation and
976 landcover-based resistance for hydrodynamic modeling of urban flooding, *Adv Water Resour*,
977 *31*, 1603-1621, DOI: 10.1016/j.advwatres.2008.07.012.
978 Skinner C. J., T. J. Coulthard, D. R. Parsons, J. A. Ramirez, L. Mullen, S. Manson. (2015), Simulating
979 tidal and storm surge hydraulics with a simple 2D inertia based model, in the Humber
980 Estuary, U.K, *Estuar Coast Shelf S*, *155*, 126-136, DOI: 10.1016/j.ecss.2015.01.019.
981 Sobol I. M. (2001), Global sensitivity indices for nonlinear mathematical models and their Monte
982 Carlo estimates, *Math Comput Simulat*, *55*, 271-280, DOI: Doi 10.1016/S0378-
983 4754(00)00270-6.
984 Tarantola S., N. Giglioli, J. Jesinghaus, A. Saltelli. (2002), Can global sensitivity analysis steer the
985 implementation of models for environmental assessments and decision-making?, *Stoch Env*
986 *Res Risk A*, *16*, 63-76, DOI: DOI 10.1007/s00477-001-0085-x.
987 Tayefi V., S. N. Lane, R. J. Hardy, D. Yu. (2007), A comparison of one- and two-dimensional
988 approaches to modelling flood inundation over complex upland floodplains, *Hydrol Process*,
989 *21*, 3190-3202, DOI: 10.1002/hyp.6523.
990 van Werkhoven K., T. Wagener, P. Reed, Y. Tang. (2008), Rainfall characteristics define the value of
991 streamflow observations for distributed watershed model identification, *Geophys Res Lett*, *35*,
992 DOI: Artn L11403

993 10.1029/2008gl034162.
994 Vrugt J. A., C. J. F. ter Braak, H. V. Gupta, B. A. Robinson. (2009), Equifinality of formal (DREAM)
995 and informal (GLUE) Bayesian approaches in hydrologic modeling?, *Stoch Env Res Risk A*,
996 *23*, 1011-1026, DOI: 10.1007/s00477-008-0274-y.

997 Warmink J. J., J. A. E. B. Janssen, M. J. Booij, M. S. Krol. (2010), Identification and classification of
998 uncertainties in the application of environmental models, *Environ Modell Softw*, *25*, 1518-
999 1527, DOI: 10.1016/j.envsoft.2010.04.011.
1000 Werner M., S. Blazkova, J. Petr. (2005), Spatially distributed observations in constraining inundation
1001 modelling uncertainties, *Hydrol Process*, *19*, 3081-3096, DOI: 10.1002/hyp.5833.
1002 Westerink J. J., R. A. Luettich, A. M. Baptists, N. W. Scheffner, P. Farrar. (1992), Tide and Storm
1003 Surge Predictions Using Finite Element Model, *Journal of Hydraulic Engineering*, *118*, 1373-
1004 1390, DOI: doi:10.1061/(ASCE)0733-9429(1992)118:10(1373).
1005 Wilson M., P. Bates, D. Alsdorf, B. Forsberg, M. Horritt, J. Melack, F. Frappart, J. Famiglietti.
1006 (2007), Modeling large-scale inundation of Amazonian seasonally flooded wetlands, *Geophys*
1007 *Res Lett*, *34*, DOI: Artn L15404

1008 10.1029/2007gl030156.
1009 Wood E. F., J. K. Roundy, T. J. Troy, L. P. H. van Beek, M. F. P. Bierkens, E. Blyth, A. de Roo, P.
1010 Doll, M. Ek, J. Famiglietti, D. Gochis, N. van de Giesen, P. Houser, P. R. Jaffe, S. Kollet, B.
1011 Lehner, D. P. Lettenmaier, C. Peters-Lidard, M. Sivapalan, J. Sheffield, A. Wade, P.
1012 Whitehead. (2011), Hyperresolution global land surface modeling: Meeting a grand challenge
1013 for monitoring Earth's terrestrial water, *Water Resour Res*, *47*, DOI: Artn W05301

1014 10.1029/2010wr010090.
1015 Yang J. (2011), Convergence and uncertainty analyses in Monte-Carlo based sensitivity analysis,
1016 *Environ Modell Softw*, *26*, 444-457, DOI: 10.1016/j.envsoft.2010.10.007.
1017 Yin J., D. P. Yu, Z. N. Yin, J. Wang, S. Y. Xu. (2013), Multiple scenario analyses of Huangpu River
1018 flooding using a 1D/2D coupled flood inundation model, *Nat Hazards*, *66*, 577-589, DOI:
1019 10.1007/s11069-012-0501-1.
1020 Yu D., S. N. Lane. (2006), Urban fluvial flood modelling using a two-dimensional diffusion-wave
1021 treatment, part 1: mesh resolution effects, *Hydrol Process*, *20*, 1541-1565, DOI:
1022 10.1002/hyp.5935.
1023 Yu D. P. (2010), Parallelization of a two-dimensional flood inundation model based on domain
1024 decomposition, *Environ Modell Softw*, *25*, 935-945, DOI: 10.1016/j.envsoft.2010.03.003.
1025 Yu D. P., T. J. Coulthard. (2015), Evaluating the importance of catchment hydrological parameters for
1026 urban surface water flood modelling using a simple hydro-inundation model, *J Hydrol*, *524*,
1027 385-400, DOI: 10.1016/j.jhydrol.2015.02.040.
1028 Zhang C., J. G. Chu, G. T. Fu. (2013), Sobol"s sensitivity analysis for a distributed hydrological
1029 model of Yichun River Basin, China, *J Hydrol*, *480*, 58-68, DOI:
1030 10.1016/j.jhydrol.2012.12.005.

1031

1032

8. Figures

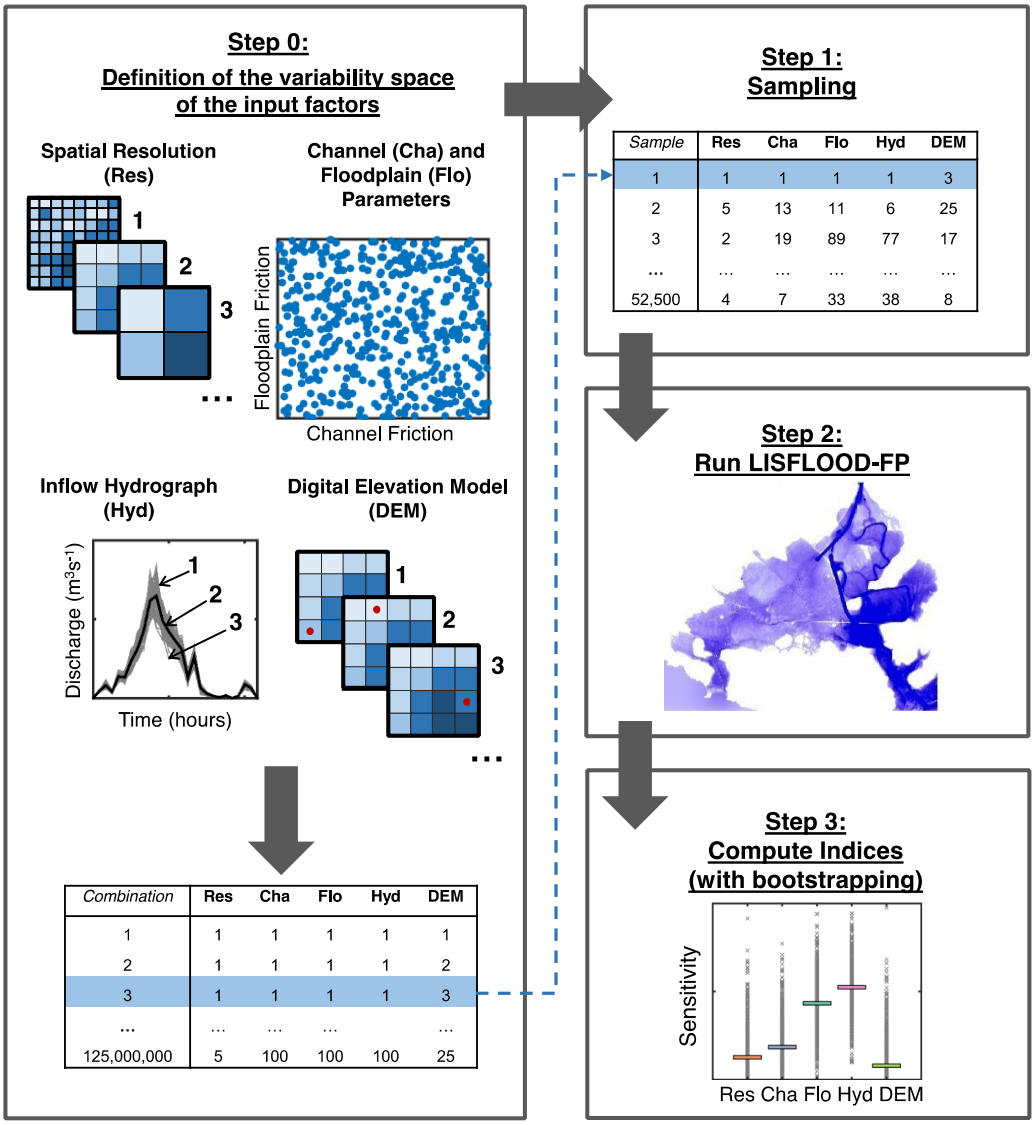

Figure 1: Flow diagram outlining the methodology utilised to perform Global Sensitivity Analysis (GSA) and to incorporate the choice of non-numerical input factors (spatial resolution and Digital Elevation Model (DEM)) in the analysis. Step 0 consists of creating a large catalogue of possible combinations of the input factors, which is then sampled from in Step 1. The flood inundation model is then run for each of these samples in Step 2 and sensitivity indices are calculated from these simulations in Step 3.

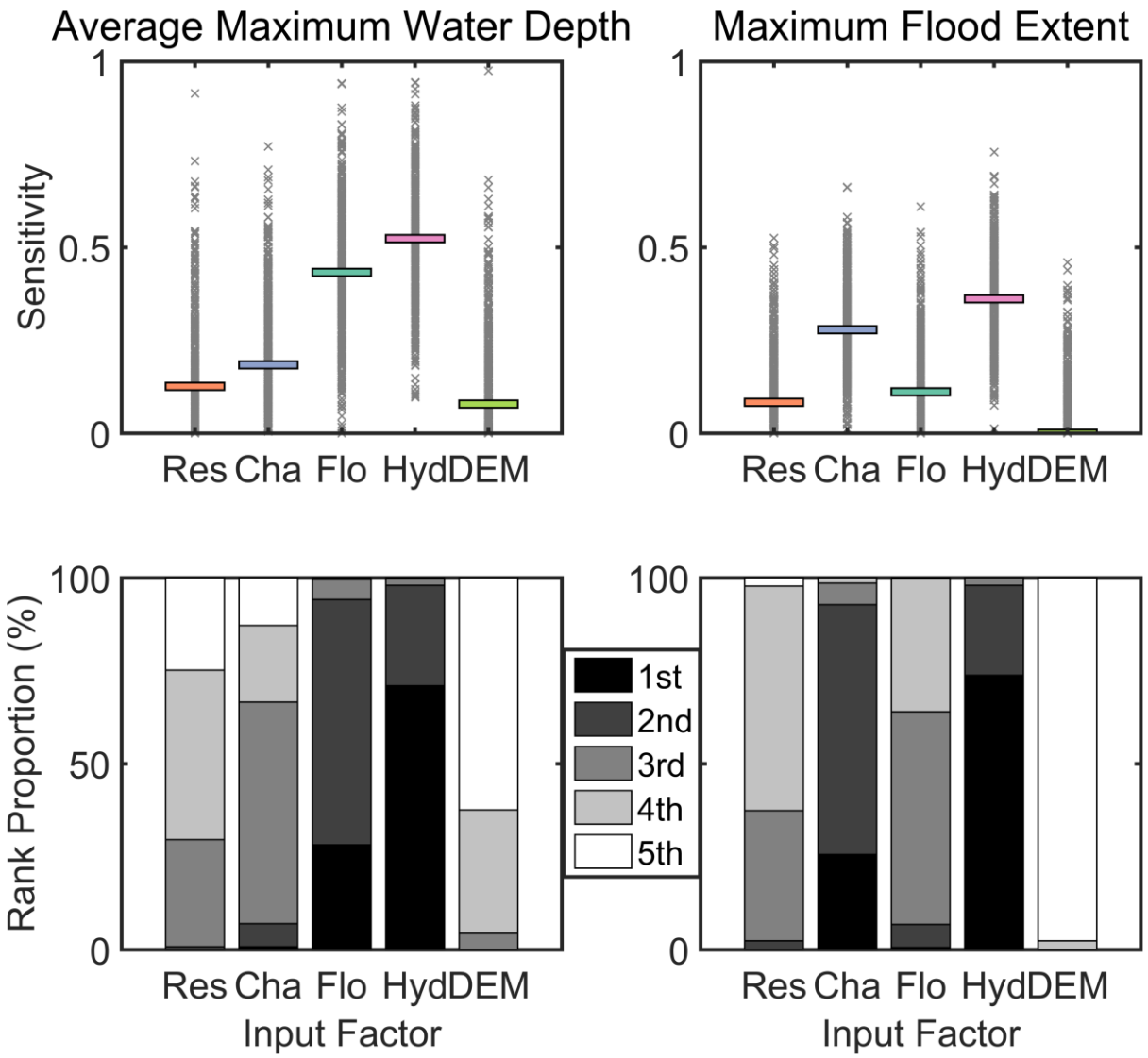

Figure 2: GSA results for two selected model outputs. The top panels show the first-order sensitivity index (or main effect) of the average maximum water depth (left) and flood extent (right) to each input factor (abbreviations are defined in Figure 1). Crosses are sensitivity index values obtained on each bootstrap resample, coloured bars are the mean values over such resamples. The bottom panels show the proportion of bootstrap resamples for which each input factor is ranked either 1st, 2nd, 3rd, 4th or 5th most influential.

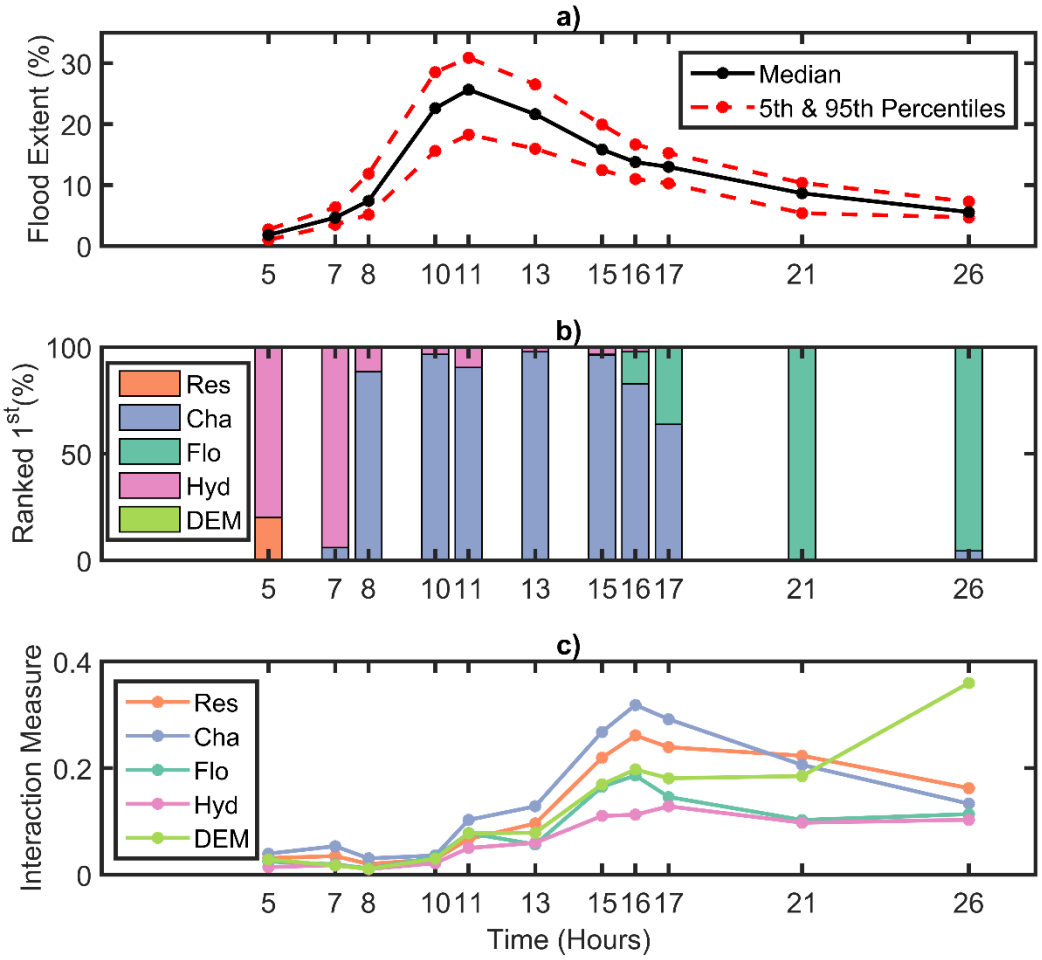

Figure 3: GSA results for flood extent during the flood simulation. a) Variation in flood extent through time as simulated by the 52,500 model realisations. The black line is the median flood extent and the dashed red lines the 5th and 95th percentiles. Flood extent is calculated as the percentage of cells classified as wet (i.e. having water depth higher than 0.10 m). b) Proportion of bootstrap resamples where an input factor was ranked most influential at each time slice. c) Interactions between input factors at each time slice. Interaction is calculated as the mean difference between the total and main effects over all bootstrap resamples. Any occurrence where such difference was negative was treated as an unreliable resample and not included in the calculation. The input factor abbreviations are defined in Figure 1.

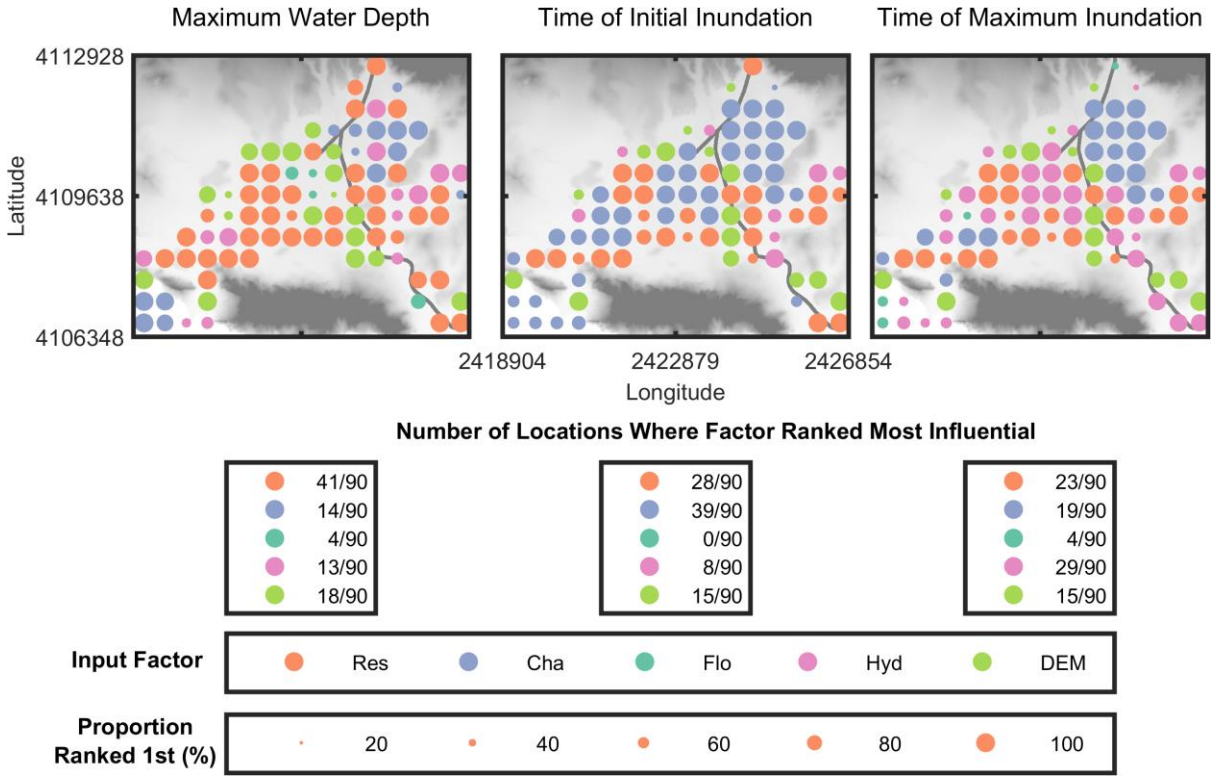

Figure 4: Nodal maps showing the spatial distribution of the most influential input factor for the maximum water depth, time of initial inundation and time of maximum inundation model outputs. The colour of the dots represents the most influential factor and the size of the dots represents the proportion of bootstrap resamples where that factor was ranked most influential. Each point is separated from one another by 500 m. The background on the plots is the 2m LiDAR DEM which has dimensions of 7.95 x 6.58 km. The input factor abbreviations are defined in Figure 1.

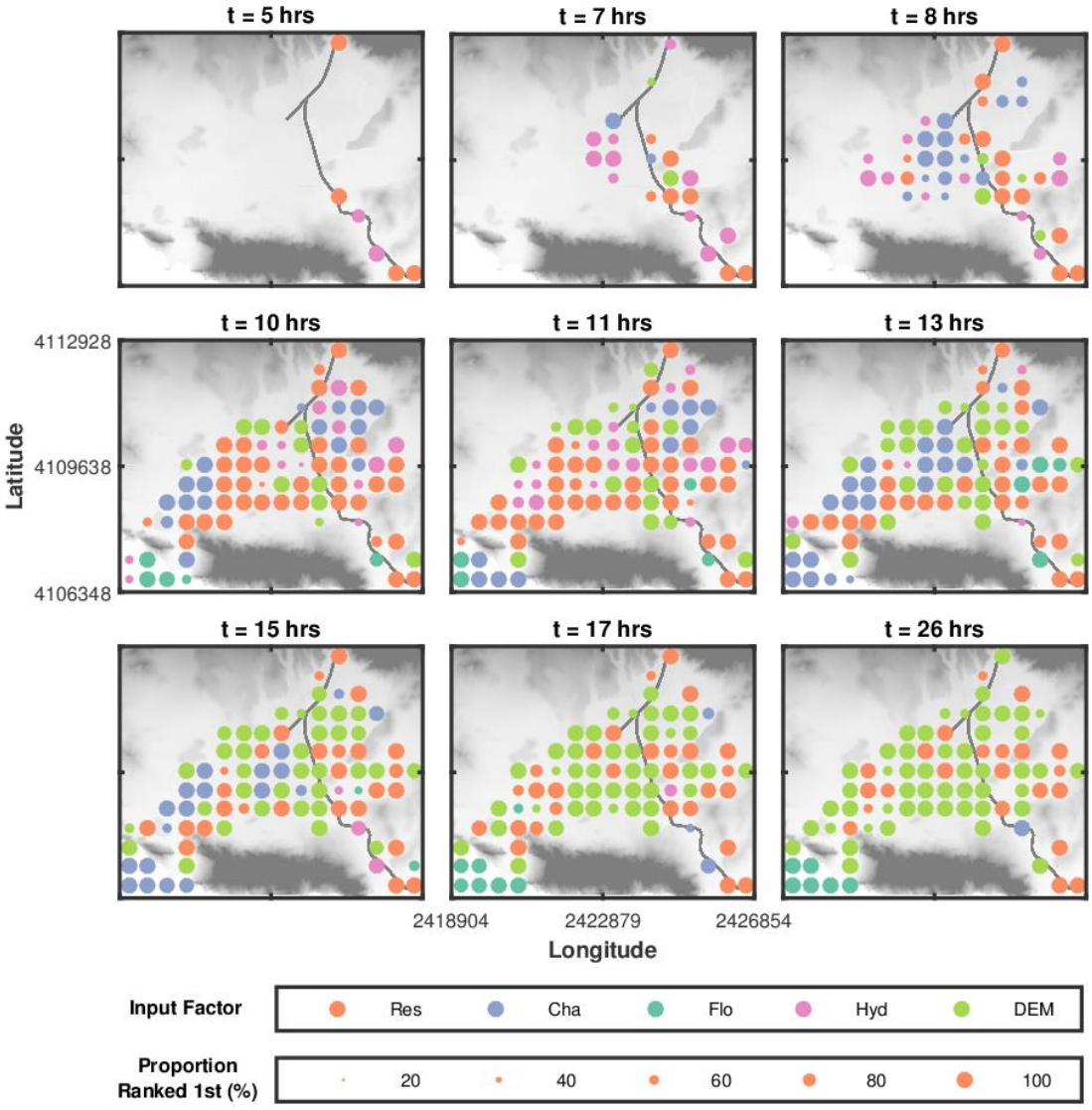

Figure 5: Nodal maps showing the spatial distribution of the most influential input factor for water depth at 9 time slices during the flood event. Meaning of colour and size of the dots, and background image as in Figure 4. Input factor abbreviations are defined in Figure 1.